Hindawi Publishing Corporation
Advances in Materials Science and Engineering
Volume 2014, Article ID 614821, 11 pages
http://dx.doi.org/10.1155/2014/614821

Research Article

Effects of Rolling Reduction and Strength of Composed Layers on Bond Strength of Pure Copper and Aluminium Alloy Clad Sheets Fabricated by Cold Roll Bonding

Yoji Miyajima, Kotaro Iguchi, Susumu Onaka, and Masaharu Kato

Department of Materials Science and Engineering, Graduate School of Science and Engineering, Tokyo Institute of Technology, 4250-J2-63 Nagatsuta-cho, Midori-ku, Yokohama 226-8502, Japan

Correspondence should be addressed to Yoji Miyajima; miyajima.y.ab@m.titech.ac.jp

Received 18 January 2014; Accepted 12 March 2014; Published 17 April 2014

Academic Editor: Roohollah Jamaati

Three types of clad sheets, Cu/Al, Cu/AA5052, and Cu/AA5083, were produced by cold roll bonding with the rolling reduction of 50% and 75%. Tensile shear tests which give tensile shear strength were performed in order to assess the bond strength. Scanning electron microscopy was performed on the fractured interface produced by the tensile shear tests, which suggests that the fracture occurs within the Al alloy layer. The tensile shear strengths considering the area fraction of deposit of Al alloy on Cu side were compared with the shear stress converting from the ultimate tensile strengths. As a result, the tensile shear strength of the clad sheets is attributed to the shear strength of Al alloy layer close to the well bonded interface. A simple model was proposed that explains the effects of the rolling reduction and area fraction of deposit of Al alloy.

1. Introduction

Composite materials which have superior characteristics compared with each composed material are widely used, and metals can be used as the composed materials. For instance, Cu/Al composites have smaller density than Cu and higher thermal and electrical conductivities than Al [1]; therefore, they are used as light weight electric wires. Such metallic composites can be fabricated by mechanical alloying, diffusion bonding, and roll bonding. Especially, roll bonding can produce large amount of metallic sheet-shaped composites, which are also called clad sheets, faster than other methods such as diffusion welding.

There are two types of roll bonding: one is hot roll bonding and the other is cold roll bonding, of which definition is that the former and the latter are carried out above and below recrystallization temperature, respectively. During hot rolling, intermetallic layers are often formed at the interfaces of clad sheets. Such intermetallic layers would reduce the bond strength for Cu/Al composites [1]. On the other hand, it is possible to form the bonding without intermetallic layers by cold roll bonding since the critical diffusion does not occur at the low process temperature.

Li et al. reviewed the bond strength of clad sheets formed by cold roll bonding for several combinations of fcc composed layers and concluded that the sufficient bonding could be achieved rather easily between fcc metallic layers [2]; Manesh prepared Al/Fe clad sheets using roll bonding and measured the bond strength by peeling tests [3]. Pozuelo et al. measured the bond strength of ultrahigh carbon steel/mild steel clad sheets by Charpy impact tests and three points bending tests. It has been reported that the higher rolling reduction and the higher surface roughness of the unrolled composed layers produce higher bond strength [4].

There are a few related models and theories for the bonding and the bond strength of clad sheets. Jamaati and Toroghinejad suggest that the faced and contaminated surface layers of metals are destroyed during roll bonding and virgin surfaces appear from the crack at the contaminated surfaces [5, 6]. Once the virgin surfaces are contacted, bonding between two metals is achieved [5, 6]. However, the relationship between the rolling reduction and the bond strength was not

Table 1: The chemical composition of AA5052 and AA5083.

Element (mass %)	Si	Fe	Cu	Mn	Mg	Cr	Zn	Al
AA5052	0.10	0.26	0.02	0.04	2.50	0.20	0.03	Bal.
AA5083	0.14	0.20	0.02	0.68	4.40	0.12	0.00	Bal.

mentioned in the paper. Le et al. reported the effect of the thickness of the surface oxide layer on Al alloys and the rolling reductions against the creation of the crack at the surface oxide layer [7], but there is no description in the case of roll bonding. Furthermore, as far as the authors know, the effect of the strength of the composed layer on the bond strength of clad sheets has not been fully understood yet.

In the present study, three types of Al alloys are chosen with strength lower than, nearly equal to, and higher than that of Cu. Using these alloy combinations, we will investigate the effect of rolling reduction and strength of composed metallic layers on bond strength of Cu/Al alloy clad sheets.

2. Materials and Methods

2.1. Materials. Materials used in the present study are pure Cu (purity of 99.99%: 4N-Cu) and three types of Al alloys (4N-Al with 99.99% purity, AA5052, and AA5083). The chemical compositions of AA5052 and AA5083 are shown in Table 1. Prior to the cold roll bonding, the alloy and metal sheets with 1 to 2 mm thickness, 70 mm width, and 150 mm length were prepared and annealed using a furnace in ambient atmosphere at 873 K for 7.2 ks for 4N-Cu and 673 K for 5.4 ks for 4N-Al, AA5052, and AA5083. Clad sheets with 1 mm thickness were made with cold rolling reductions r (%) of either 50% (1 mm thick sheets) or 75% (2 mm thick sheets).

2.2. Cold Roll Bonding. Although there are many parameters affecting cold roll bonding such as rolling conditions, shape factor in rolling, surface conditions, adsorbed contaminants, oxide films, surface preparation methods, lubricant conditions, and postheat treatments [2], a specific cold rolling condition for accumulative roll bonding (ARB) process with lubrication is treated in this paper. It is noted that the lubrication condition was achieved by using machine oil.

The ARB process is one of the severe plastic deformation processes which allows giving large amount of plastic strain for metallic sheets in order to fabricate ultrafine grains (UFGs) [8, 9]. The procedure of cold roll bonding used in this study is almost the same as that used in the ARB process. The cold roll bonding consists of three steps. First, the surface of annealed sheets was cleaned using acetone, and a side of the sheets was surface treated by a wire-brash. Secondly, a 4N-Cu sheet and an Al alloy sheet were stacked, and then four holes at the four corners are created using a drill. Then, the two metal sheets were tied by metallic wires. Thirdly, roll bonding was achieved using a rolling mill of which diameter of rolls is 250 mm with a roll speed of 21 rpm and two types of the rolling reductions r; one is 50% and the other is 75%. Here, it should be pointed out that 50% of rolling reduction was performed by one path of rolling, whereas 75% of rolling was carried out by three paths in order to reduce the process heat and protect the rolling mill. The average strain rate for the roll bonding is between $10\,s^{-1}$ and $30\,s^{-1}$. Here, the average strain rate is equivalent to strain divided by time of rolling. As a result, clad sheets consisting of two metallic layers are fabricated.

The effective prevention of heat generation is very important since the temperature increase may create intermetallic layers between the metal sheets which would deteriorate the bond strength. Here, the sample coordination was defined as rolling direction (RD), normal direction (ND), and transverse direction (TD).

Judging from the fact that the length of the plates after 50% and 75% of rolling reduction became almost twice and four times, respectively. Therefore, the plastic deformation during the cold rolling can be approximated as the plane strain compression along ND and the length change along TD can be neglected.

The combinations of the metal sheets were 4N-Cu/4N-Al, 4N-Cu/AA5053, and 4N-Cu/AA5083. Thus, there are six types of samples with regard to the combination of the metals and the thickness reduction. Hereby, the samples are denoted as combination of metals and the thickness reduction, such as Cu/Al-50% and Cu/AA5052-75%. Here, it should be noted that the thickness reduction values have a scatter of about a few percent, but this amount of difference in the thickness reduction did not affect the Vickers hardness H_v of the metal sheet. Thus, nominal thickness reduction values are used in this study.

2.3. Mechanical Tests. Vickers hardness tests were carried out using micro-Vickers hardness machine MXT-α1 (Matsuzawaseiki) with the load of 300 gf. The specimens for Vickers hardness tests were cut from metal sheets using a wire-electric discharge machine. The planes normal to the TD of the sheets were used for the Vickers hardness tests. The surface of the specimens was polished mechanically and finished by buffing with 1 μm diamond liquid (Refinetech). Seven points on the cut specimen were used for measuring Vickers hardness per one specimen, and the average of five values of H_v excluding the highest and the lowest values was treated as the H_v of the specimen. In the case of the roll bonded specimens, the metal layers were chosen for the measurement points. In this manner, it was confirmed that a few % difference in r does not affect the H_v of composed layers after cold roll bonding as mentioned before.

Two types of mechanical tests, uniaxial tensile tests and tensile shear tests, were performed using a tensile test machine NMB TG-50 kN (Minebea) at room temperature (R.T.). Specimens for the uniaxial tensile tests were cut using the wire-electric discharge machine, and the surface of the specimens was mechanically polished using SiC paper up

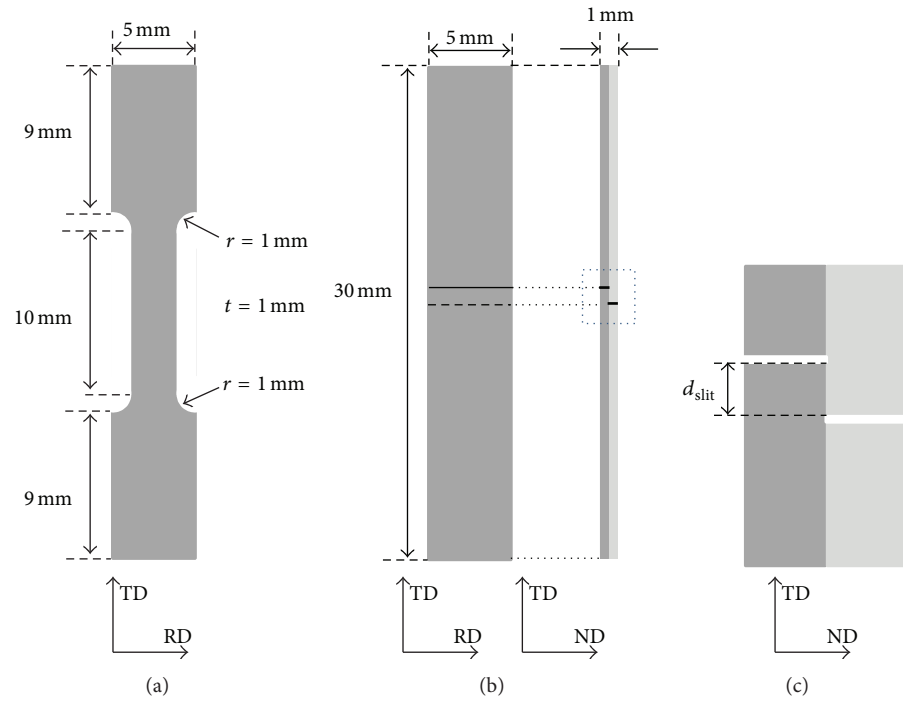

Figure 1: Schematic illustrations of (a) a specimen for the uniaxial tensile test and (b) a specimen for tensile shear test. (c) The magnified schematic illustration of (b) indicated as square dot lines in (b).

to #4000. As shown in Figure 1(a), the gage length, width, and thickness were 10 mm, 3 mm, and 1 mm, respectively. The tensile direction was along TD, and the initial strain rate of the uniaxial tensile tests was 8.3×10^{-5} s^{-1}. Some single layer specimens were obtained from the clad sheets using mechanical polishing, and they are denoted such like Cu-Cu/Al-50% and AA5052-Cu/AA5052-75%. The specimens for the tensile shear tests were cut using the wire-electric discharge machine to be rectangular shapes of which dimensions were 30 mm of length, 5 mm of width, and 1 mm of thickness as shown in Figure 1(b). The surface of the specimens was mechanically polished using SiC paper up to #1000, and then two slits are fabricated by the wire-electric discharge machine as shown in Figure 1(c). The distance between the two slits d_{slit} is different for each sample in order to limit the maximum applied load during tensile shear tests. Because when the applied stress exceeds the yield stress of remained layer at the two slits, bending occurs at the slit and accurate tensile shear tests cannot be performed. The details of the specimens for tensile shear tests are listed in Table 2.

2.4. Observations of Fractured Interfaces. After the tensile shear tests, the surfaces of destroyed roll bonded interface were observed by a digital microscope VHX-500 (Keyence). Backscattered electron image (BEI) of some delaminated surfaces were obtained using a scanning electron microscope (SEM) JSM-7001F (JEOL) with a field emission gun and an acceleration voltage of 15 kV. It was also confirmed by energy dispersive X-ray spectrometry (EDS) JED-2300 equipped in another SEM JSM-7100F (JEOL) that the difference of contrast on BEIs was due to the difference of metals. Two-dimensional EDS mappings were performed with the acceleration voltage and the illumination current of 15 keV and 1.8 nA. The data analysis was performed using a software analysis station (JEOL). As a result, the bright and the dark regions on the fracture interfaces were attributed to Cu and Al alloy regions, respectively. Image thresholding was applied for obtained BEIs, and the area fractions of Cu and Al alloy regions were evaluated.

Table 2: Details of the specimens for tensile shear tests.

Sample name	Width, w/mm	width of slits, d_{slit}/mm	Area of bonding, S/mm^2
Cu/Al-50%	4.73	0.35	1.66
Cu/Al-75%	4.73	0.34	1.61
Cu/AA5052-50%	4.73	0.75	3.55
Cu/AA5052-75%	4.73	0.55	2.60
Cu/AA5083-50%	4.73	0.75	3.55
Cu/AA5083-75%	4.73	0.55	2.60

3. Results and Discussion

3.1. Uniaxial Tensile Tests of Annealed Metal Sheets. As shown in Figure 2, true stress versus true strain (s-s) curves of annealed composed sheets (4N-Cu, 4N-Al, AA5052, and AA5083) are obtained using uniaxial tensile tests. The curves were drawn with an assumption that the gage of the tensile

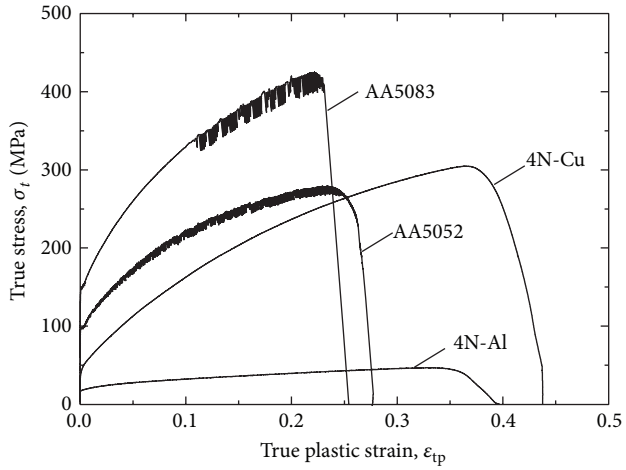

Figure 2: s-s curves of the annealed sheets.

specimens deforms uniformly under constant volume condition. It should be noted that the above assumption is not satisfied once necking occurs after true stress reaches ultimate tensile strength (UTS), but such plastic instability region of s-s curves should be treated as advisory values.

As can be seen, AA5083 has the highest yield stress followed in order by AA5052, 4N-Cu, and 4N-Al. After work hardening, ultimate tensile strength (UTS) of 4N-Cu becomes comparable to that of AA5052 and total elongation is the largest in 4N-Cu.

AA5000 series is a well-known Al-Mg solid solution strengthening type alloy, and the difference of the concentration of Mg affects the mechanical properties. Actually, the UTS of AA5083 is higher than that of AA5052. A part of the s-s curves of AA5052 and AA5083 shows serration which is associated with dynamic strain aging [10].

3.2. Uniaxial Tensile Tests of Clad Sheets and Composed Layer. Figure 3 shows s-s curves of the clad sheets and the composed layers for (a) Cu/Al-50%, (b) Cu/Al-75%, (c) Cu/AA5052-50%, (d) Cu/AA5052-75%, (e) Cu/AA5083-50%, and (f) Cu/AA5083-75%. These curves show work-softening, which is attributed to the necking. From the s-s curves, 0.2% proof stresses, the UTS of the clad sheets, and the composed layers are evaluated as shown in Figures 4 and 5, respectively. The s-s curves of the clad sheets are displayed until a composed layer reaches to fracture since the cross sectional area of the sheet suddenly drops, and it is difficult to use them even for advisory for trend since the assumption for the s-s curves is uniform elongation under constant volume condition. In the case of Cu/Al clad sheets, there is not clear fracture of a composed layer so that whole s-s curves are displayed.

All Cu layers and Al layers show the ductile s-s curves, whereas AA5052 and AA5083 layers fracture suddenly after they reach the plastic instability region. It is similar to the case of the s-s curves of the annealed AA5052 and AA5083 sheets which also fracture suddenly as shown in Figure 2.

From the deformation stress point of view, the s-s curves of Cu/Al and Cu/AA5052 clad sheets seem to be almost the average of the s-s curves of composed layers. On the other hand, it is not clear to discuss the deformation stress of Cu/AA5083-50% and Cu/AA5083-75% since the deformation stresses of the clad sheets are comparable with either the Cu or the AA5083 layers.

Nevertheless, the clad sheets can be considered to be composite consisting of two layers. If the fractions of the cross-sectional area which are being normal to the tensile direction of composed Cu and Al alloy layers are A_{Cu} and A_{Al}, respectively, the average stress σ_{compo} can be written as [11–13]

$$\sigma_{\mathrm{compo}} = A_{\mathrm{Cu}} \cdot \sigma_{\mathrm{Cu}} + A_{\mathrm{Al}} \cdot \sigma_{\mathrm{Al}}. \quad (1)$$

Here, σ_{Cu} and σ_{Al} are the stresses of Cu and Al alloy layers, respectively. The thickness of the Cu and Al alloy layers are almost the same in this study, and therefore, the values of the 0.2% proof stress and the UTS of the clad sheets and their composed layers are reasonable. The 0.2% proof stress and the UTS of the all composed layers increase with increasing r, which is associated with work hardening of the composed layers during the rolling.

3.3. Tensile Shear Tests of Clad Sheets. Figure 6 shows the results of the tensile shear test of the clad sheets. The left and the right column show load F versus crosshead displacement x and shear stress τ versus crosshead displacement x, respectively. Here, τ was evaluated using F and the area of bonding S with an equation $\tau = F/S$. The top, the middle, and the bottom rows show the results of Cu/Al, Cu/AA5052 and Cu/AA5083 clad sheets, respectively.

The F-x curves of the same clad sheet with 50% and 75% rolling reduction show similar gradient at the initial elastic stage of tensile shear tests for all the clad sheets. If the dominant elastic deformation occurs at the noncut layer at the two slits, it can be understandable. The thickness of all the composed layers is about 0.5 mm and the width of the specimens is the same as shown in Table 2, and the elastic modulus is insensitive to the degree of deformation. Thus, the gradient at the initial elastic stage of F-x curves tends to be the same when the uncut composed layers at two slits deform elastically. However, when x exceeds at a certain point, the F-x curves become different.

The trends after the elastic region are classified to be two types: one is Cu/Al and the others are Cu/AA5052 and Cu/AA5083. In the former case, F increases with increasing x and reaches to the maximum value of F, and then F gradually decreases towards zero with increasing x. In the latter case, F increases and then reaches to a plateau with increasing x. Finally, the specimen suddenly fractures with increasing x.

The τ-x curves clearly show the effect of r for the bond strength as shown in the right column of Figure 6. The higher r increases both the apparent shear tensile strength τ_a, which is the maximum τ, and fracture elongation for all the specimens.

3.4. Observation of Fractured Interfaces. The fractured interface was observed using SEM after the tensile shear tests. It is worthwhile to emphasize that the BEIs of Cu side seem to be

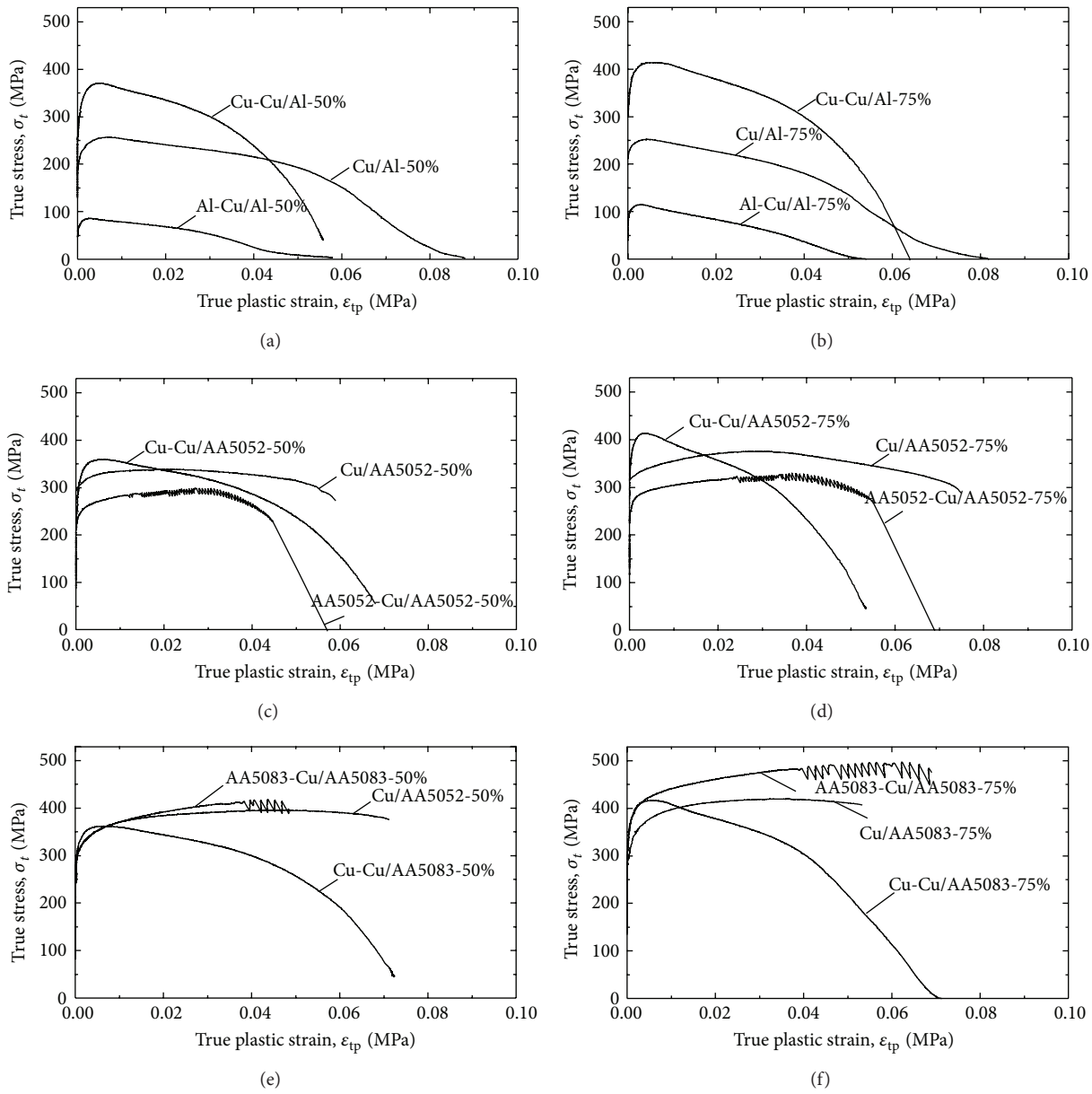

Figure 3: s-s curves of the clad sheets and the composed layers. (a) Cu/Al-50%, (b) Cu/Al-75%, (c) Cu/AA5052-50%, (d) Cu/AA5052-75%, (e) Cu/AA5083-50%, and (f) Cu/AA5083-75%.

partly covered by Al alloy, whereas BEIs of the Al alloy side seem to be only Al alloy. Although the morphology of Cu side is different among all the samples, the morphology of Al alloy side is almost the same as shown in Figure 7. The bright and dark regions correspond to Cu and Al alloys, respectively, as mentioned in materials and methods section.

Thus, only the BEIs of Cu side are shown in Figure 8 and discussed in this paper. The morphology of deposit of Al alloys on Cu side is elongated along TD and separated along RD when r is 50%. When r is 75%, larger area seems to be covered compared with that in the case of 50%. Especially, the most area on the Cu side of Cu/Cu-75% seems to be covered by Al.

Image thresholding was applied to the BEIs and the area fraction of Al deposit on Cu side ρ was evaluated as shown in Figure 9(a). The higher r results in the higher ρ. It can be also said that the higher strength of composed Al alloy layer results in the smaller ρ, especially at higher r. The deposit of Al alloy on Cu side indicates that the Al alloy was deformed by tensile shear tests and the fracture occurs within the Al alloy layer.

As shown in Figure 9(b), apparent tensile shear strengths τ_a can be evaluated from τ-x curves, but ρ should be taken into account for the tensile shear strength if the tensile shear strengths are attributed to the shear deformation of Al alloy layer. The corrected tensile shear strengths τ_c are evaluated

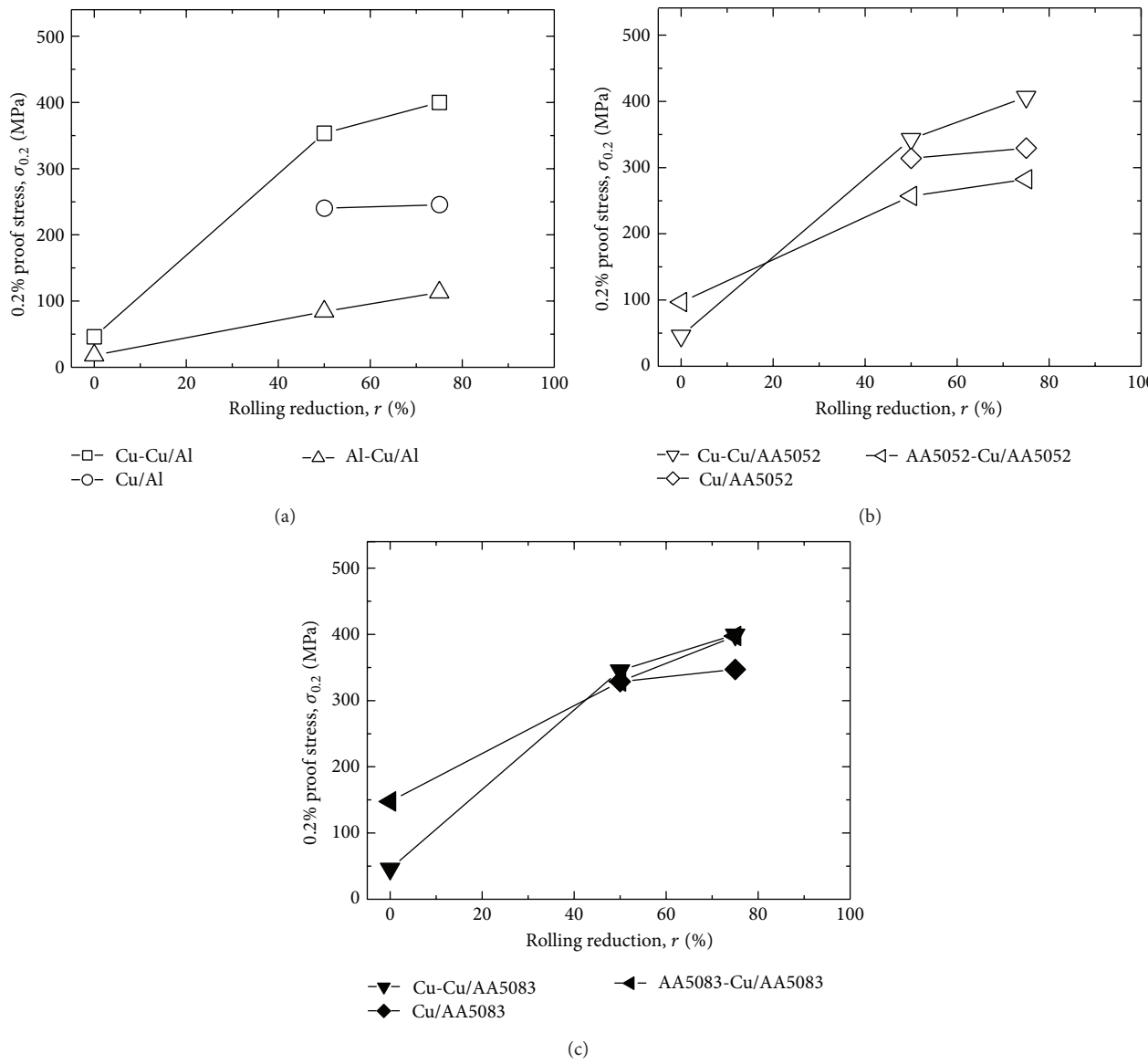

Figure 4: Rolling reduction dependence on the 0.2% proof stress of (a) the Cu/Al clad sheet and the composed layer, (b) the Cu/AA5052 clad sheet and the composed layers, and (c) the Cu/AA5083 clad sheet and the composed layers.

from τ_a using $\tau_c = \tau_a/\rho$, as displayed in Figure 9(b). It should be emphasized that the τ_c is treated as the bond strength in this study.

The shear strength of Al alloy layers can be converted from the UTS of Al alloy layers using the following assumption. Von Mises's equation allows to convert three-dimensional stress condition to uniaxial tress condition [14]:

$$\overline{\sigma} = \sqrt{\frac{1}{2}\left\{(\sigma_1 - \sigma_2)^2 + (\sigma_2 - \sigma_3)^2 + (\sigma_3 - \sigma_1)^2\right\}}. \quad (2)$$

Uniaxial stress condition means $\sigma_1 = \tau$, $\sigma_3 = \sigma_2 = 0$, and therefore, (2) can be rewritten as follows:

$$\overline{\sigma} = \sigma. \quad (3)$$

On the other hand, pure shear stress condition means $\sigma_1 = -\sigma_2 = \tau$, $\sigma_3 = 0$, and therefore, (2) can be rewritten as follows:

$$\overline{\sigma} = \sqrt{3}\sigma. \quad (4)$$

Using (4), the UTS of Al alloy layers can be converted to shear strength τ_{UTS} as displayed in Figure 9(b).

τ_{UTS} and τ_c are comparable values in the case of 75% rolling reduction, whereas τ_c is almost twice as high as τ_{UTS} in the case of 50% of rolling reduction. The higher rolling reduction (r = 75%) is thought to form large area of stronger bond strength at the interface between Cu and Al alloy layers. Therefore, actual fracture occurs within Al alloy layer during the tensile shear tests in the case of r = 75%, and weak bonded area does not affect τ_c. On the other hand, the lower rolling reduction (r = 50%) is thought to form small area fraction

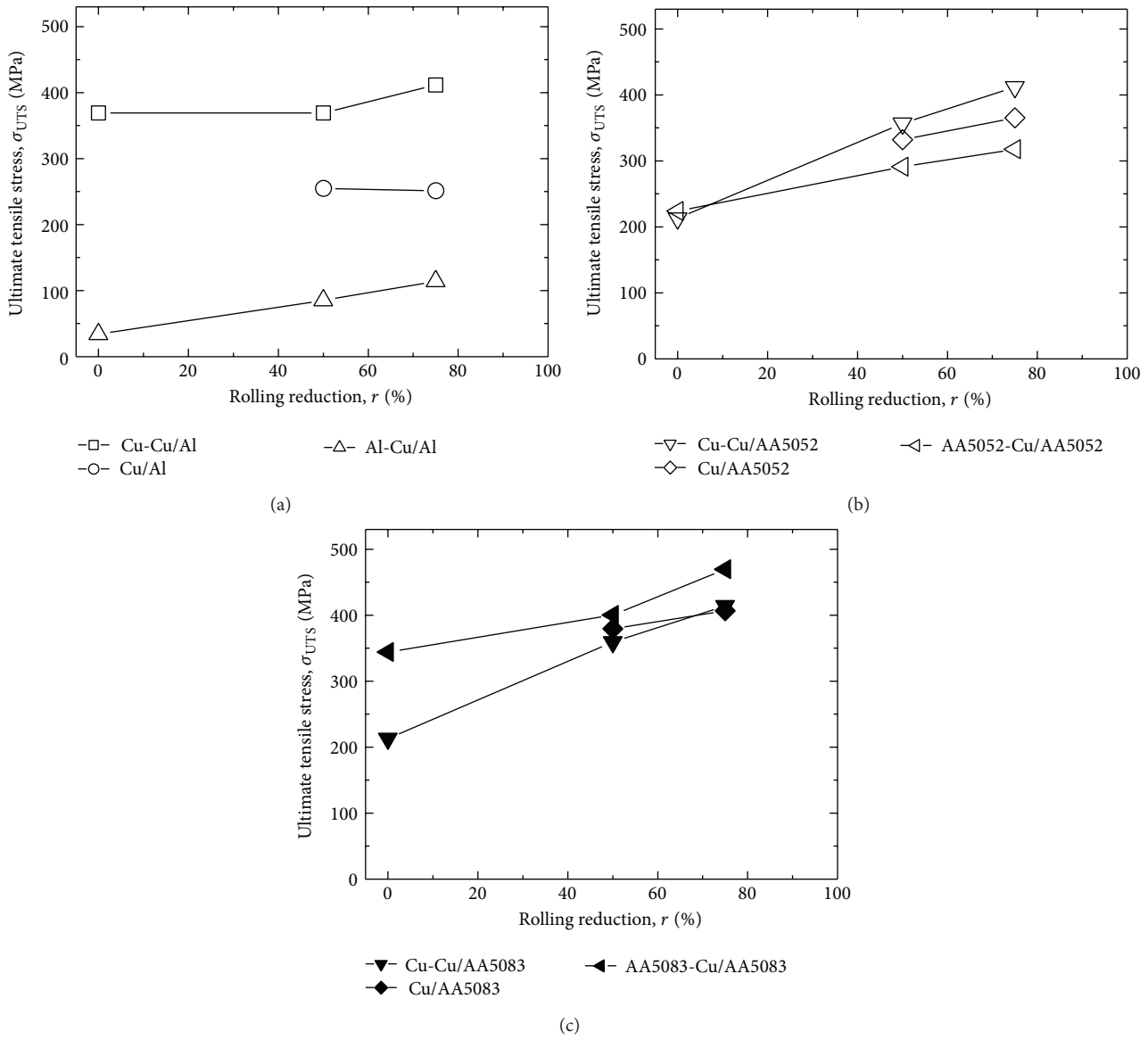

Figure 5: Rolling reduction dependence on the ultimate tensile stress of (a) the Cu/Al clad sheet and the composed layer, (b) the Cu/AA5052 clad sheet and the composed layers, and (c) the Cu/AA5083 clad sheet and the composed layers.

of well bonded area, and therefore, separation at the weakly bonded interface during the tensile shear tests also affects the τ_a. Consequently, τ_c is overestimated.

3.5. Proposed Model. In order to understand the above results about ρ, a model is proposed with three assumptions as follows. First, the surface of annealed metals is covered by surface layer such as native oxide. Secondly, the surface layer is perfectly brittle, and therefore, no plastic deformation occurs at the surface layer. Thirdly, the bonding between different metals occurs only when the virgin surfaces contact each other. If these assumptions are satisfied, the surface brittle layer is destroyed during roll bonding and virgin surface appears from the cracks elongated along TD.

Figure 10 is the schematic illustration close to the interface before and after the cold roll bonding which is based on the proposed model. Three types of interface can be assumed in Figure 11; type-A interface is not a bonded interface, type-B interface is a well bonded interface, and type-C interface is a weakly bonded interface. Metallic bonding is expected only at the type-B interface. When tensile shear tests are performed, shear deformation occurs within Al alloy layer close to the well bonded type-B interface, and deposit of Al alloy on the Cu side is observed. This is the reason why the deposit of Al is elongated along TD and separated along RD.

Strictly speaking, the separation of deposit also occurs along TD if the BEIs are carefully checked, which can be also understood by the proposed model since there is small elongation along TD about 1.5 % after roll bonding.

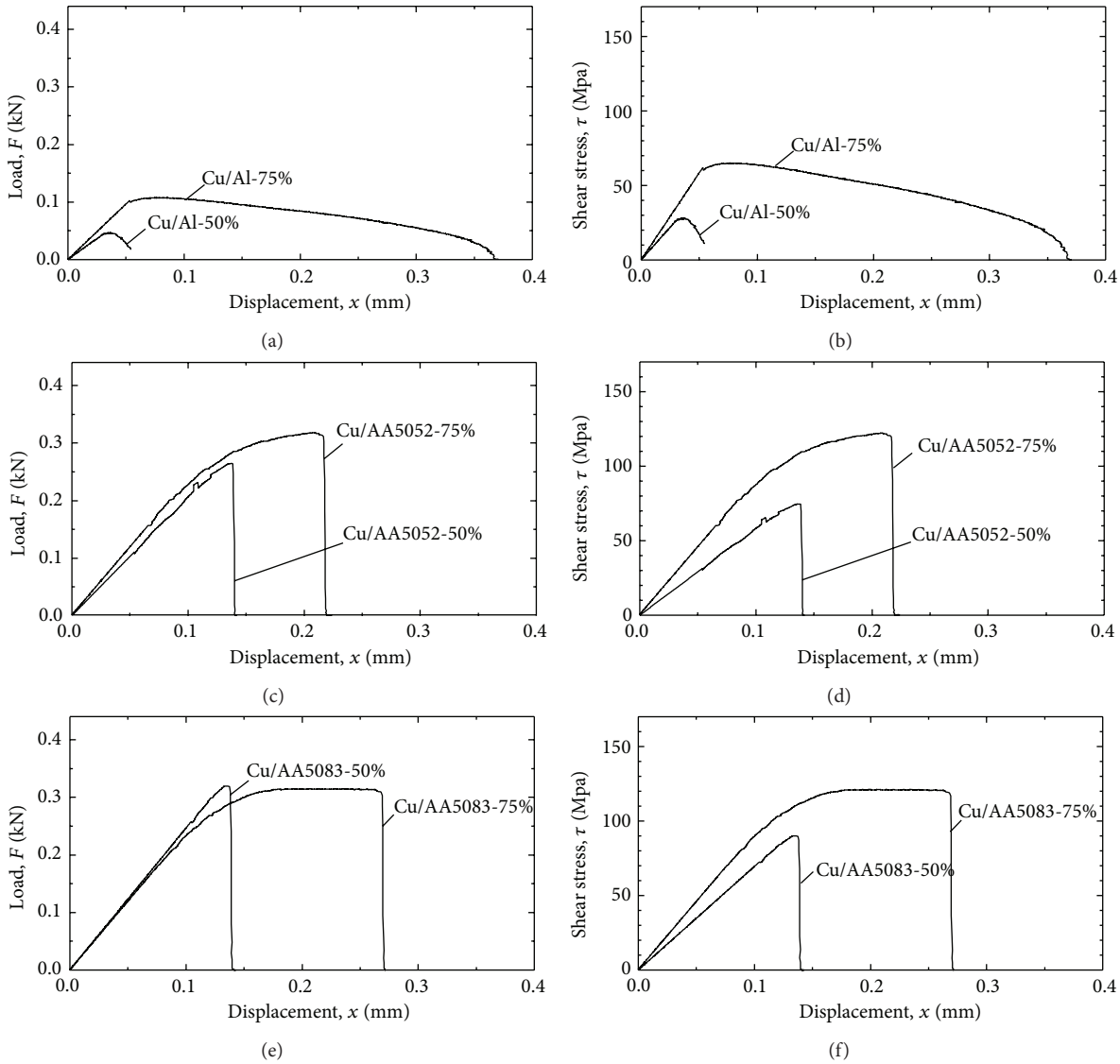

Figure 6: Results of tensile shear tests, (a) and (b) are Cu/Al-50% and Cu/Al-75%, (c) and (d) are Cu/AA5052-50% and Cu/AA5052-75%, and (e) and (f) are Cu/AA5083-50% and Cu/AA5083-75%. Left and right column represent load-displacement curves and shear stress displacement curves, respectively.

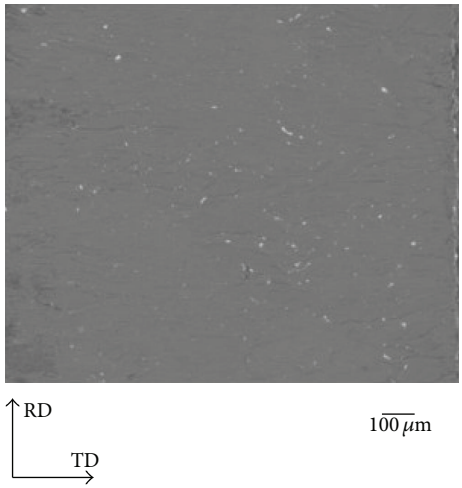

Figure 7: Fractured interface of Al alloy side after a tensile shear test.

3.6. Relationship between Area Fraction of Deposit and Rolling Reduction. Experimental results show the higher r results in the larger ρ. In other words, the higher r results have a larger possibility of forming well bonded type-B interface. Simple equations are used to explain the results quantitatively.

Let us consider the plastic deformation of one composed layer before and after rolling reduction. Here, we assume that the layer satisfies constant volume condition and ideal plane strain compression. Thus, (5) is satisfied. Consider the following:

$$L_0 t_0 = L_1 t_1. \tag{5}$$

Here, L_0 and t_0 are the length and the thickness of the sheet before rolling, respectively. L_1 and t_1 are the length and thickness of the layer after rolling, respectively. The surface layer is again assumed to be perfectly brittle, and therefore, the total length of surface layer is also L_1 before and after roll

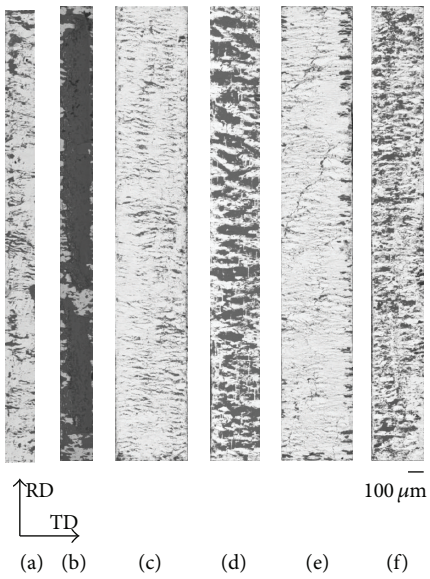

Figure 8: Fractured interface after tensile shear tests, (a) Cu/Al-50%, (b) Cu/Al-75%, (c) Cu/AA5052-50%, (d) Cu/AA5052-75%, (e) Cu/AA5083-50%, and (f) Cu/AA5083-75%.

bonding. Thus, the expected probability of virgin surface P_v can be described as follows using (5):

$$P_v = \frac{L_1 - L_0}{L_1} = 1 - \frac{L_0}{L_1} = 1 - \frac{t_1}{t_0}. \quad (6)$$

Here, r is defined as

$$r = 100 \times \left(\frac{t_0 - t_1}{t_0} \right) = 100 \times \left(1 - \frac{t_1}{t_0} \right). \quad (7)$$

Equation (8) can be derived from (6) and (7) as follows:

$$P_v = r. \quad (8)$$

Equation (8) also indicates that higher r expects larger P_v, obviously.

If the virgin surface appears completely randomly after roll bonding, the expected probability of well bonded type-B interface P_e is simply written as follows:

$$P_e = P_{v,\mathrm{Cu}} \times P_{v,\mathrm{Al}} = r_{\mathrm{Cu}} \times r_{\mathrm{Al}} = r^2. \quad (9)$$

Here, $P_{v,\mathrm{Cu}}$ and $P_{v,\mathrm{Al}}$ are P_v for Cu and Al alloy, respectively. r_{Cu} and r_{Al} are the rolling reductions of Cu and Al alloy layers, respectively. r_{Cu} and r_{Al} are almost the same as $r = 0.5$ for this study.

Figure 10 shows the relationship between ρ and r. The dashed line represents the expected ρ following equation (9). Almost all ρ seem to locate on or close to the dashed line, and therefore, the proposed model can explain the situation used in this study. However, the result of Cu/Al-75% deviates from the predicted line based on the simple model. It can be attributed to the large elongation on the s-s curve of Al-Cu/Al-75%. During the tensile shear test of Al layer of Cu/Al-75%, large elongation is expected for the Al layer. Then, the undeposited area can be covered by the elongated Al, and the area of deposit of Al is overestimated.

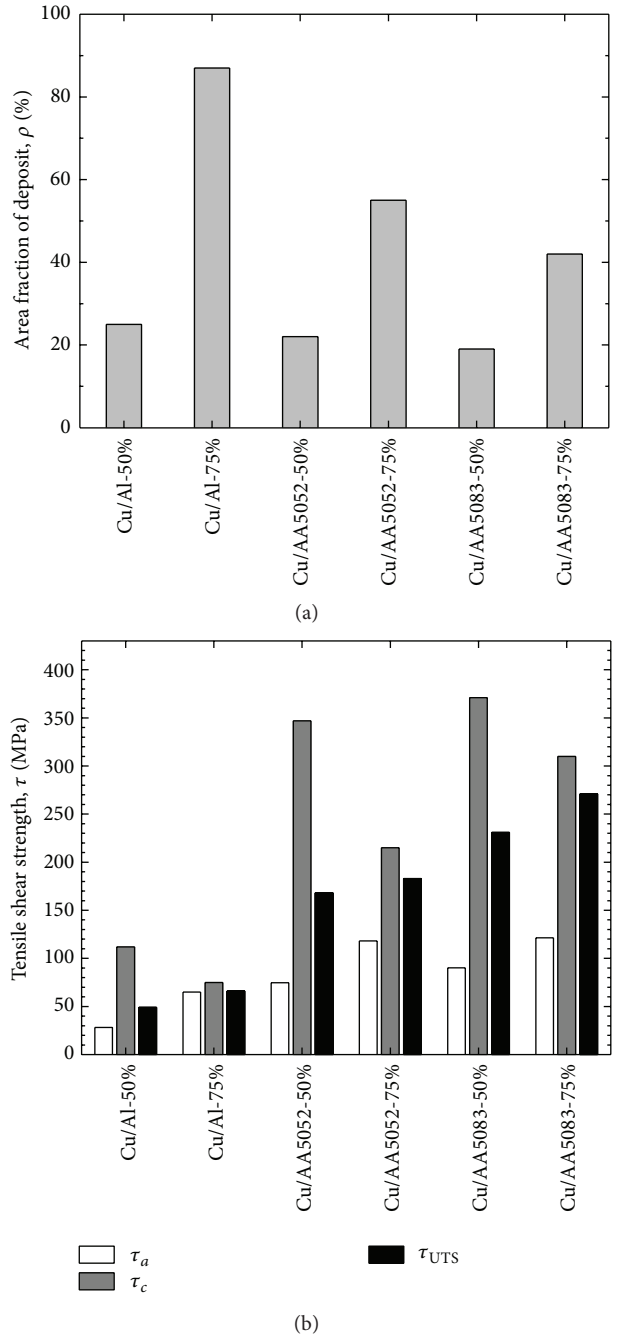

Figure 9: (a) Area fraction of deposit and (b) apparent tensile shear strengths obtained from tensile shear tests, corrected tensile shear strength with considering the area fraction of deposit on the fracture interface, and tensile shear strengths converted from the ultimate tensile strength of the Al alloy layers for Cu/Al-50%, Cu/Al-75%, Cu/AA5052-50%, Cu/AA5052-75%, Cu/AA5083-50%, and Cu/AA5083-75%.

4. Conclusions

In this study, three types of clad sheets: Cu/Al, Cu/AA5052, and Cu/5083 were fabricated by cold roll bonding with the rolling reduction of 50% and 75%. The tensile shear tests were performed in order to measure the bond strength. SEM

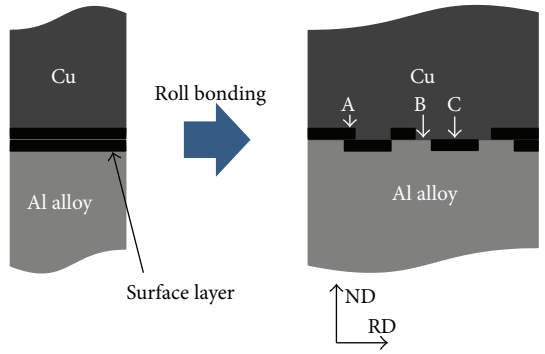

Figure 10: A schematic illustration of interface before and after cold roll bonding. Three types of interface can be assumed: type A, B, and C interfaces. They are indicated by arrows. Only Type B becomes a well-bonded interface.

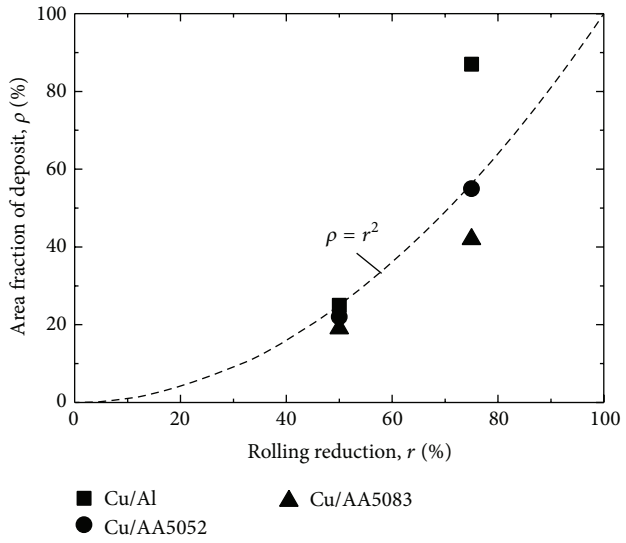

Figure 11: Area fraction of deposit versus rolling reduction. Dashed line represents the estimated values following the proposed model.

observations revealed that the fracture occurs within the Al alloy layer close to the interface. Thus, the part of the fracture interface on the Cu side was covered by the Al alloy after the tensile shear tests. The area fraction of Al alloy deposit on the Cu side was measured. If the rolling reduction is the same, the area fraction of the deposit increases with decreasing strength of the Al alloy layer. All the clad sheets show larger area fraction of deposit at 75% of rolling reduction compared with that at 50% of rolling reduction. The difference in tensile shear strength, which is considered to be the bond strength of clad sheets, can be understood by considering both the strength of composed layers and the area fraction of deposit. The relationship between the area fraction of deposit and the rolling reduction can be explained by a simple model proposed in this study.

Conflict of Interests

The authors declare that there is no conflict of interests regarding the publication of this paper.

Acknowledgments

This study was financially supported by a Grant-in-aid for Scientific Research on Innovative Area "Bulk Nanostructured Metals" no. 22102006 through the Ministry of Education, Culture, Sports, Science, and Technology (MEXT), Japan. The authors are most grateful to Professor Eiichi Sato, Japan Aerospace Exploration Agency (JAXA), for the use of the rolling mill in his laboratory.

References

[1] W. Xie, T. Yamaguchi, and K. Nishio, "Formation of intermetallic phases on the bond interface of aluminum-clad copper," *Journal of the Japan Institute of Metals*, vol. 75, no. 3, pp. 166–172, 2011.

[2] L. Li, K. Nagai, and F. X. Yin, "Progress in cold roll bonding of metals," *Science and Technology of Advanced Materials*, vol. 9, no. 2, Article ID 023001, 2008.

[3] H. D. Manesh, "Assessment of surface bonding strength in Al clad steel strip using electrical resistivity and peeling tests," *Materials Science and Technology*, vol. 22, no. 6, pp. 634–640, 2006.

[4] M. Pozuelo, F. Carreno, and O. A. Ruano, "Delamination effect on the impact toughness of an ultrahigh carbon-mild steel laminate composite," *Composites Science and Technology*, vol. 66, no. 15, pp. 2671–2676, 2006.

[5] R. Jamaati and M. R. Toroghinejad, "High-strength and highly-uniform composite produced by anodizing and accumulative roll bonding processes," *Materials & Design*, vol. 31, no. 10, pp. 4816–4822, 2010.

[6] R. Jamaati and M. R. Toroghinejad, "The role of surface preparation parameters on cold roll bonding of aluminum strips," *Journal of Materials Engineering and Performance*, vol. 20, no. 2, pp. 191–197, 2011.

[7] H. R. Le, M. P. F. Sutcliffe, P. Z. Wang, and G. T. Burstein, "Surface oxide fracture in cold aluminium rolling," *Acta Materialia*, vol. 52, no. 4, pp. 911–920, 2004.

[8] Y. Saito, H. Utsunomiya, N. Tsuji, and T. Sakai, "Novel ultra-high straining process for bulk materials development of the accumulative roll-bonding (ARB) process," *Acta Materialia*, vol. 47, no. 2, pp. 579–583, 1999.

[9] Y. Saito, N. Tsuji, H. Utsunomiya, T. Sakai, and R. G. Hong, "Ultra-fine grained bulk aluminum produced by accumulative roll-bonding (ARB) process," *Scripta Materialia*, vol. 39, no. 9, pp. 1221–1227, 1998.

[10] A. H. Clausen, T. Borvik, O. S. Hopperstad, and A. Benallal, "Flow and fracture characteristics of aluminium alloy AA5083-H116 as function of strain rate, temperature and triaxiality," *Materials Science and Engineering A*, vol. 364, no. 1-2, pp. 260–272, 2004.

[11] I. W. Chen, E. J. Winn, and M. Menon, "Application of deformation instability to microstructural control in multilayer ceramic composites," *Materials Science and Engineering A*, vol. 317, no. 1-2, pp. 226–235, 2001.

[12] S. L. Semiatin and H. R. Piehler, "Deformation of sandwich sheet materials in uniaxial tension," *Metallurgical Transactions A*, vol. 10, no. 1, pp. 85–96, 1979.

[13] S. L. Semiatin and H. R. Piehler, "Formability of sandwich sheet materials in plane strain compression and rolling," *Metallurgical Transactions A*, vol. 10, no. 1, pp. 97–107, 1979.

[14] M. Kato, S. Onaka, and S. Kumai, *Zairyokyodogaku*, Asakura, Tokyo, Japan, 1999.